Supplementary material of the manuscript "Probabilistic projection of sea-level change along the world's coastlines" submitted to Earth System Dynamics

Perrette et al. (2011)

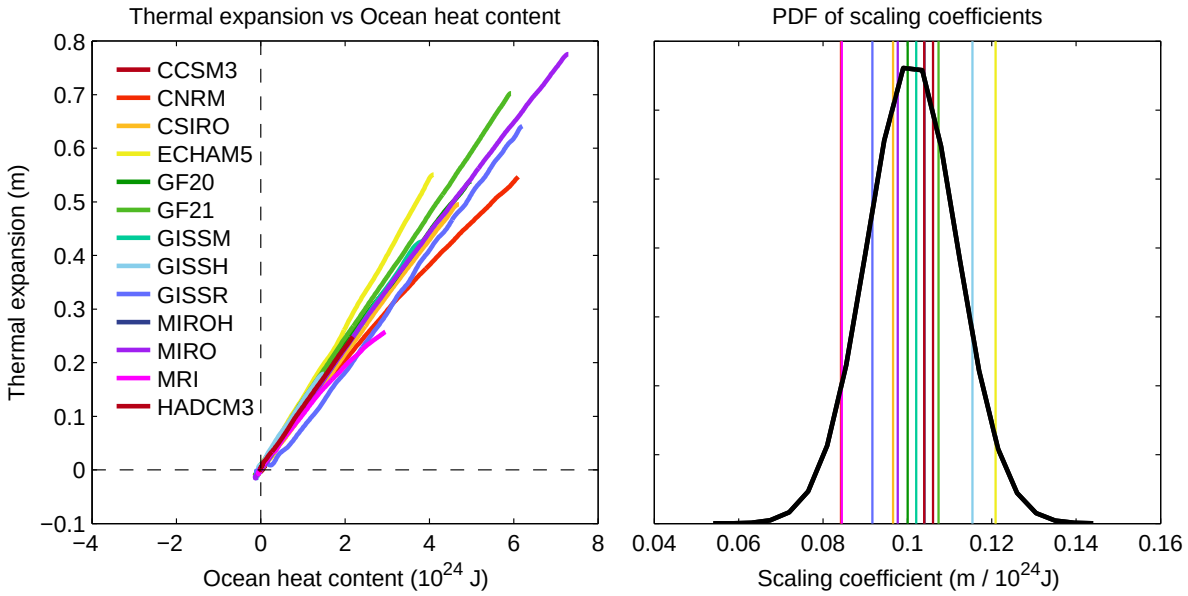

Figure S1: Global mean thermal expansion vs. ocean heat uptake in a sample of CMIP3 GCMs (left) and actual values of the corresponding regression coefficients with the fitted Gaussian distribution used for deriving thermal expansion by scaling MAGICC6 ocean heat uptake results.

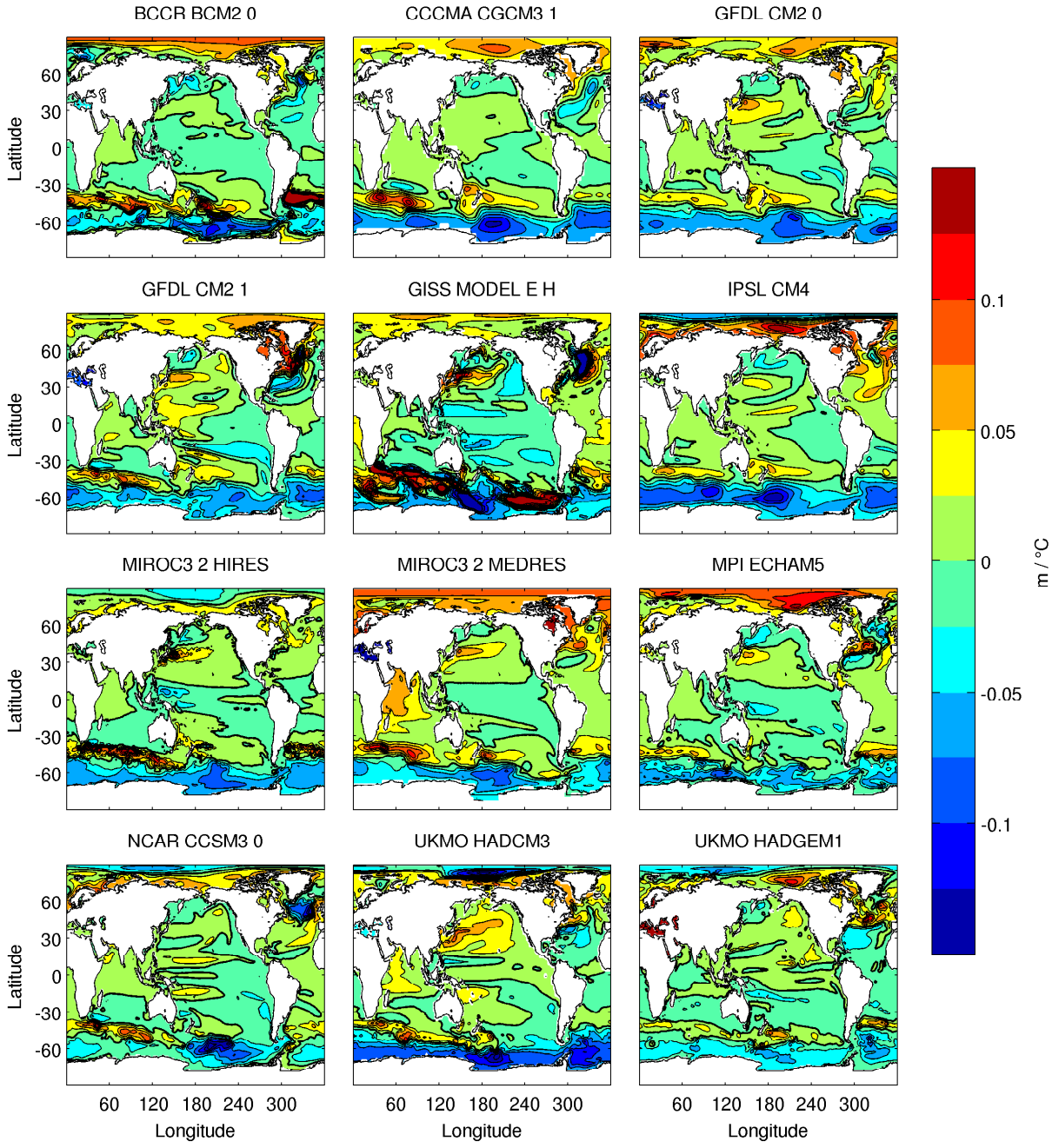

Figure S2: Regression coefficients of dynamic sea-level change against global mean temperature anomaly (in m.K^{-1}) for the SRES A1B scenario over the 2000-2100 period. Contour line intervals are 0.025 m.K^{-1}

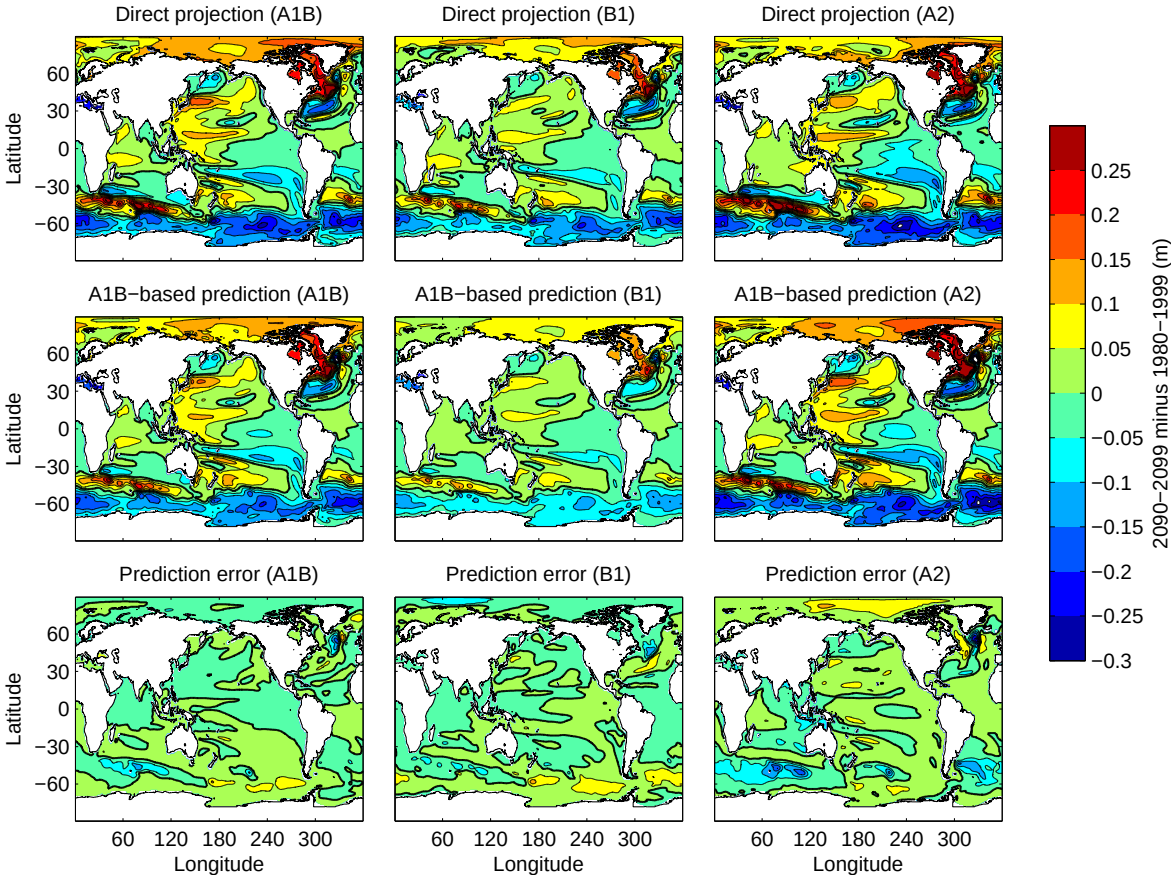

Figure S3: Comparison between direct model projections (GFDL CM2.1) between 1980-1999 and 2090-2099 averages (top) with predicted patterns using the regression method (middle), for the SRES scenarios A1B, B1, and A2 (from left to right). The difference between the predicted and projected values is also shown (bottom). Note that the predictions always use the same regression pattern derived from A1B scenario.

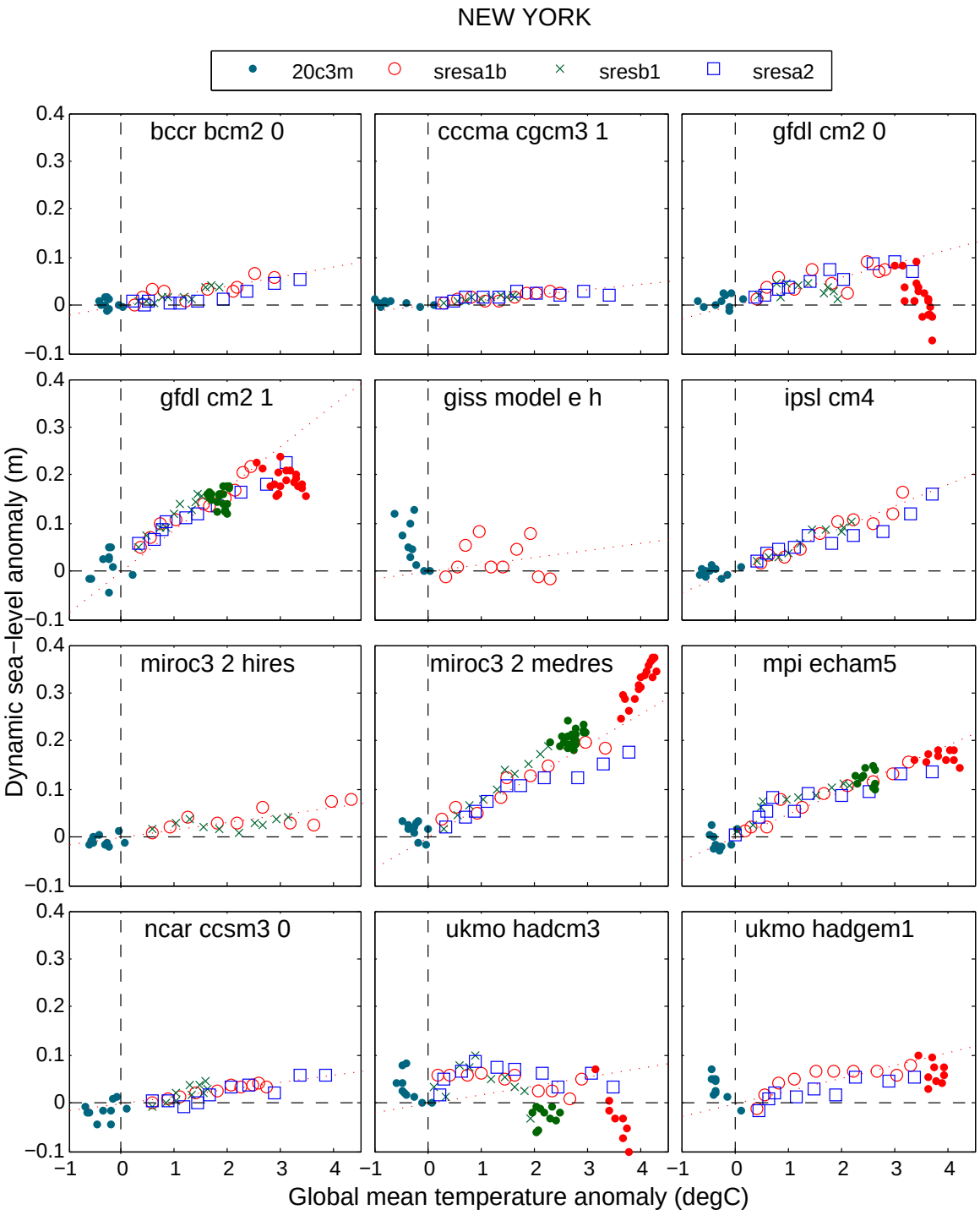

Figure S4: Scatter plot of dynamic sea-level anomaly in New York City region against global mean surface air temperature anomaly (with respect to a 1980-1999 reference period). The data represent three SRES scenarios (A1B, B1, A2) and a simulation of the 20$^{\text{th}}$ century (20c3m), as indicated in the legend. The red and dark green dots correspond to the stabilization period of the A1B and B1 scenarios (after 2100), respectively. During the stabilization period the linear relationship between dynamic sea-level change and global mean temperature is less robust, but this does not affect our projections, which focus on the end of the 21$^{\text{st}}$ century. The markers are 10-year averages. The dotted line is a linear regression over 2000-2100 for the SRES A1B scenario using yearly values, as used to derive patterns of figure Figure S2. The data are retrieved as an average within 200km of the geographical coordinates [40.5N, 73.5W] on models own grids.

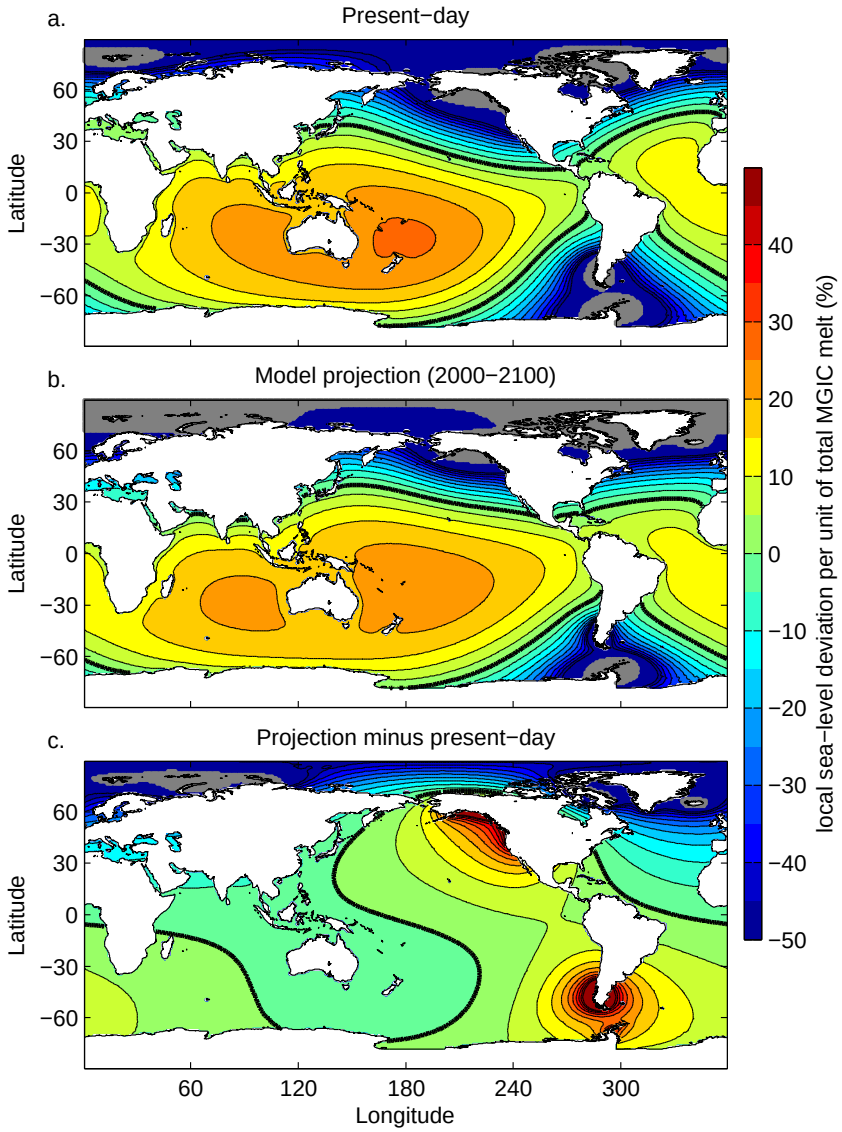

Figure S5: MGIC gravitational fingerprints (in % of total MGIC source spread uniformly across the oceans) computed after (a) observations from Bamber and Riva (2010) (except for the Asian high mountains region which is based on Jacob et al. (2012)) and (b) Radic and Hock (2011) model simulations of 21st century MGIC loss (the fingerprint used in this study). (c) Difference between (b) and (a) (both were normalized beforehand as on the figure, because only relative loads are important for our scaling approach). Contour line intervals are every 10%. The thick black line indicates the global mean sea-level change. Gray area is less than -100%, meaning sea-level fall.

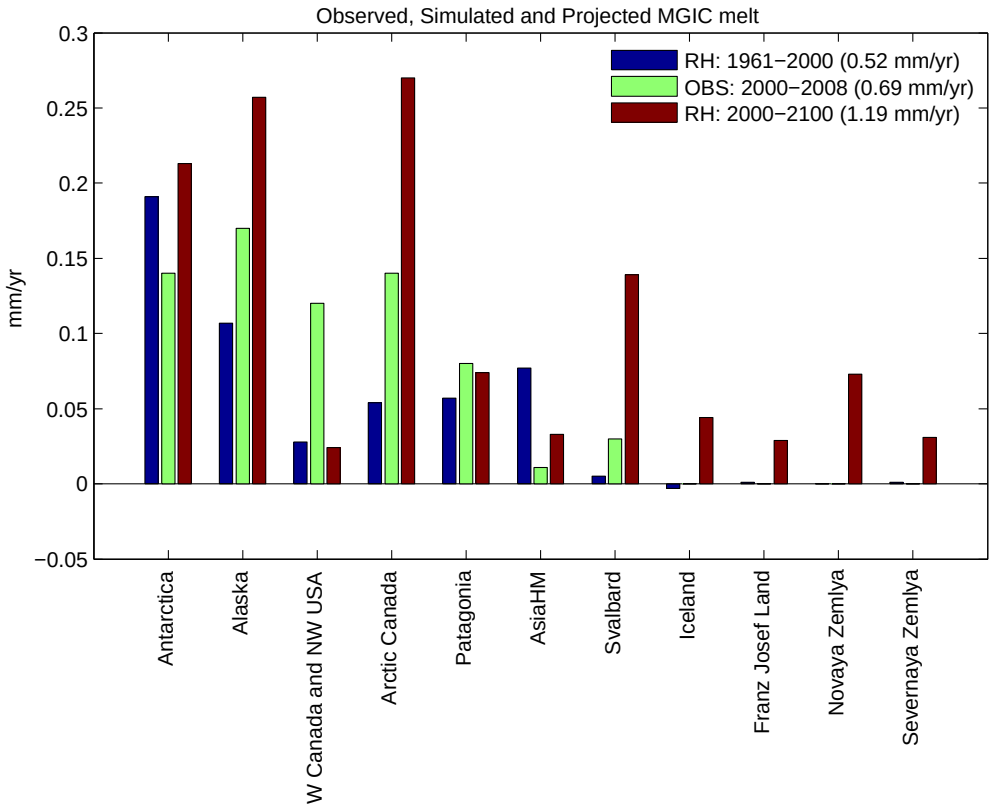

Figure S6: MGIC contribution to SLR as simulated for the past 1961-2000 period (Radic and Hock, 2011, thereafter RH11) (blue), observed over the recent 2000-2008 period (Bamber and Riva (2010), except for Asian high mountains which is based on Jacob et al. (2012)) (green) and projected over the 2000-2100 period (RH11) (red). In RH11, the 1961-2000 period actually corresponds to the calibration period, and is therefore very close to observed, ground-based MGIC evolution during this time interval. This shows that projected future MGIC melt is generally consistent with the observed trend (monotonic, increasing contributions of MGIC with time), with the notable exception of Western Canada and North Western USA, Asian high mountains and Antarctica Peninsula regions. The non-monotonic trends for these regions can likely be explained by inconsistencies between past and present data (model simulation calibrated to ground-based measurements for 1961-2000, and mostly a compilation of satellite remote sensing measurements for 2000-2008, respectively) or by model short-comings (missing processes, incomplete data for the calibration). We considered the generally monotonic trend and the large (yet presently unobserved) expected MGIC melt in the Northern Atlantic and Arctic Ocean as a compelling argument for using model-based rather than present-day observations to create our MGIC gravitational fingerprints. RH11 data obtained from their table S6.

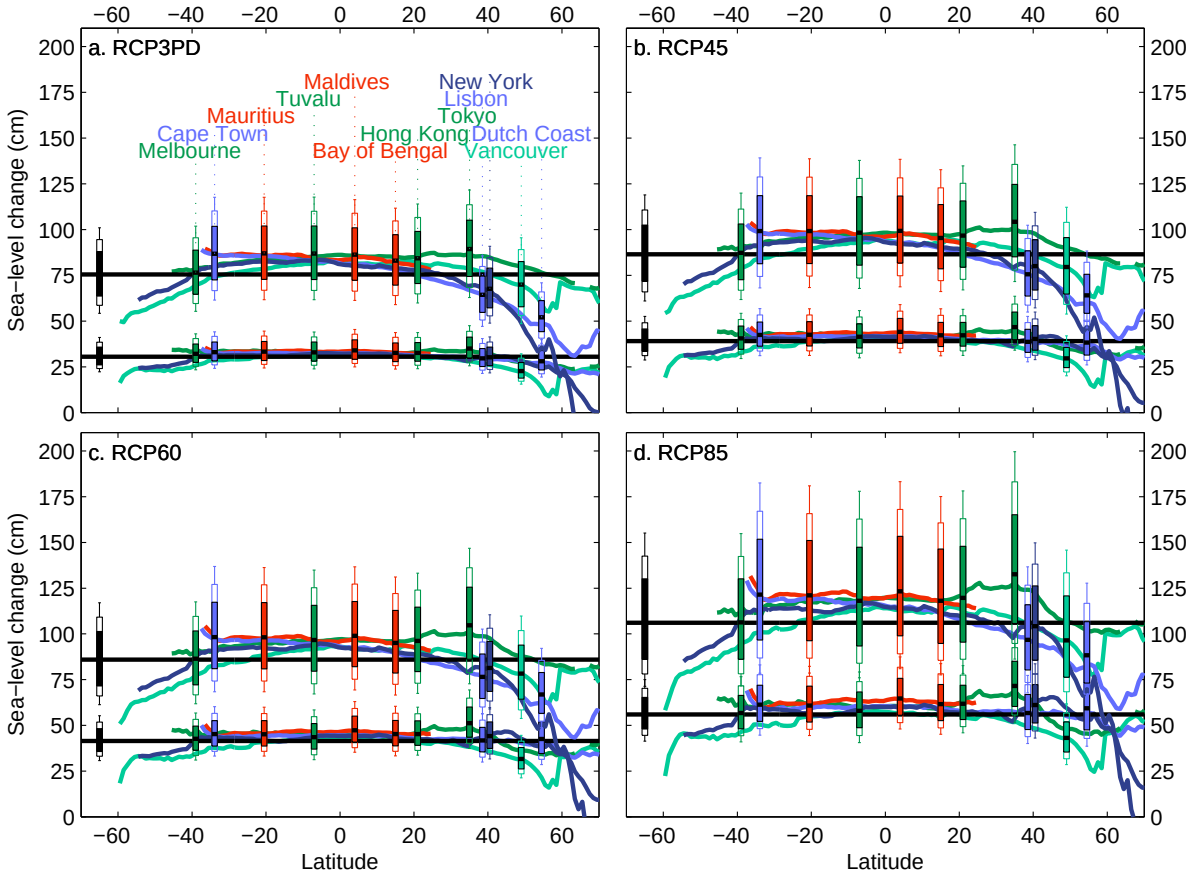

Figure S7: Sea-level change along the world's coastlines for the four RCP scenarios (a-d) with two ice-sheet cases per panel (IPCCAR4^{+}: bottom and "top-down": top), between 1980-1999 and 2090-2099. The legend is the same as Figure 3 of the main document, except that error bars describe here the absolute sea-level change, expressed in cm.

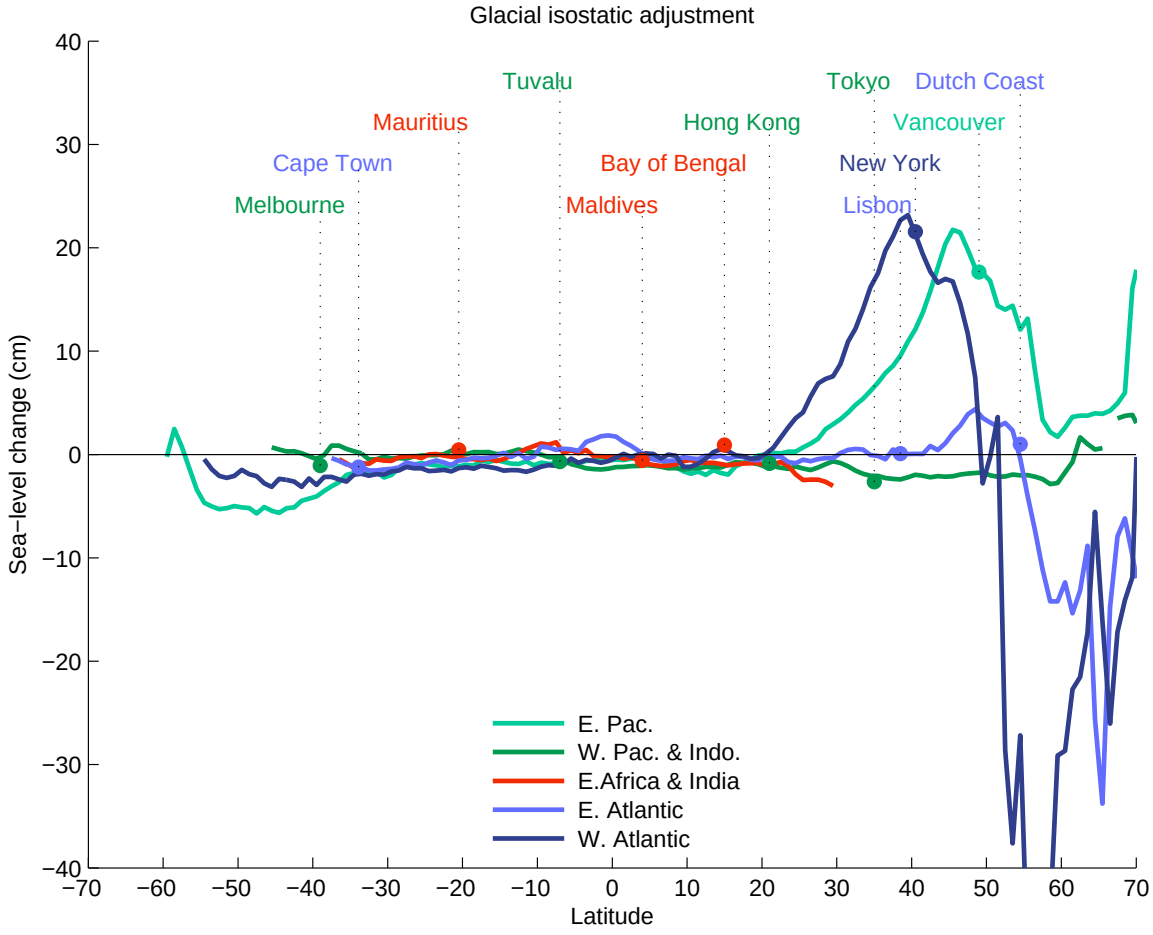

Figure S8: Glacial isostatic adjustment expressed as sea-level change along the world's coastlines, between 1980-1999 and 2090-2099. The data is averaged over a 300 km wide band of coastal waters. Based on ICE-5G (VM2) Peltier (2004).

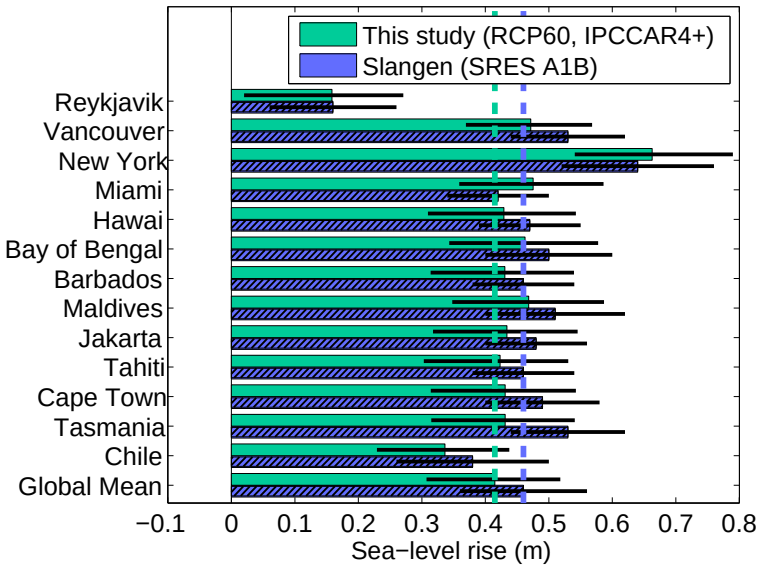

(a) Total SLR

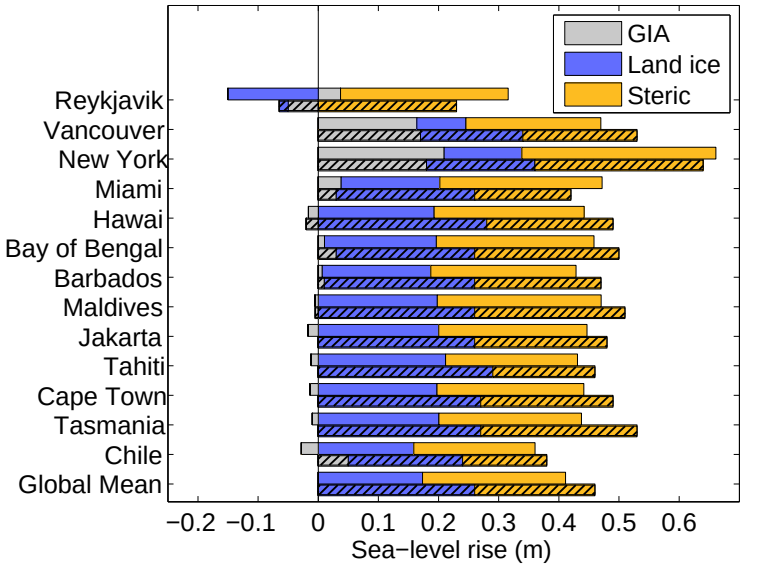

(b) Individual contributions

Figure S9: Comparison of the IPCCAR+ ice-sheet case (with the RCP 6.0 emission scenario) (filled) with regional SLR projections from Slangen et al. (2011) (with the SRES A1B emission scenario) (hatched). (a) Total SLR with 16^{th}-84^{th} (this study) and 1-sigma uncertainties (Slangen) (both uncertainty measures are equivalent for a Gaussian distribution). (b) Individual contributions to SLR. GIA is included in this figure, to ease comparison (in both cases based on the ICE-5G (VM2) model, but with slightly different implementations). The dashed vertical line in (a) indicated the global mean SLR. The RCP 6.0 emission scenario is comparable to SRES A1B, and the IPCCAR4+ ice sheet case is siremilar to Slangen et al's treatment of the ice sheets (except that they do consider negative AIS SMB and add a dynamic ice-sheet contribution based on the IPCCAR4 on top of GIS and AIS contribution, which leads to slightly higher ice-sheet contributions than our approach of setting Antarctica contribution to zero and ignoring any dynamic contribution from the ice sheets to SLR). These differences in treatment of the the ice sheets, as well as slighly higher MGIC contributions in Slangen et al. (2011) than in our approach, explain the overall higher land-ice contribution in Slangen et al. (2011). Location coordinates may differ between both studies, which is an additional source of discrepancy in regions with small-scale SLR features. We choose this combination of emission scenario and ice-sheet case from our results to help focusing on the regional distribution of SLR. Figures 3 and S7 show a more comprehensive comparison between ice-sheet cases and emission scenarios.

Table S1: Global statistics for the linear regression of dynamic sea-level against global mean temperature. The table indicates for each model, and for each SRES scenario, the global mean temperature (column name: "GMT"), global mean thermal expansion ("TSL"), and the spatial average of the normalized prediction error between 1980-1999 and 2090-2999 (difference between prediction from the regressed A1B pattern and direct model projection, both in absolute value). The prediction error is expressed in % of the direct model projection, and is averaged with appropriate area-weighting. A negative sign indicates that our temperature-based prediction tends to underestimate the projected local changes (regardless of their direction). The averaging domain is global but only comprehends the grid cells where local dynamic sea-level is greater than 5 cm (labelled ">5cm") or greater than 10 cm (labelled ">10cm"), which are of greatest interest, and which avoids division by zero. Missing values correspond to missing simulations in CMIP3.

SRES scenario	B1				A1B				A2			
Model code	GMT (°C)	TSL (cm)	>5cm (%)	>10cm (%)	GMT (°C)	TSL (cm)	>5cm (%)	>10cm (%)	GMT (°C)	TSL (cm)	>5cm (%)	>10cm (%)
BCCR BCM2.0	1.8		-22	-20	2.9		3	2	3.4		0	15
CCCMA CGCM3.1	1.6	23	-19	-20	2.5	29	-7	1	3.4	34	0	17
GFDL CM2.0	1.9	17	-49	-30	2.8	22	-4	-2	3.3	23	-5	-11
GFDL CM2.1	1.5	18	-25	-28	2.4	23	-12	-16	3.1	25	-2	-8
GISS-EH					2.3	17	-2	-4				
IPSL CM4	2.2		-23	-21	3.2		-1	-7	3.7		-9	-10
MIROC3.2 HIRES	3.1	22	-6	-8	4.3	29	0	0				
MIROC3.2 MEDRES	2.3	21	-29	-17	3.3	27	-7	-8	3.8	28	0	-1
MPI ECHAM5	2.2	19	-12	-12	3.3	24	-3	-5	3.7	25	-2	0
NCAR CCSM3.0	1.6	18	-28	-31	2.7	25	-8	-14	3.9	29	0	1
UKMO HADCM3	1.9	15	-23	-23	2.9	21	3	0	3.5	23	15	6
UKMO HADGEM1					3.3		-5	-7	4.1			
Multi-model mean	2.0	19	-24	-21	3.0	24	-4	-5	3.6	27	0	1

References

Bamber, J. and Riva, R.: The sea level fingerprint of recent ice mass fluxes, The Cryosphere, 4, 621–627, doi:10.5194/tc-4-621-2010, URL http://www.the-cryosphere.net/4/621/2010/, 2010.

Jacob, T., Wahr, J., Pfeffer, W. T., and Swenson, S.: Recent contributions of glaciers and ice caps to sea level rise., Nature, 482, 514–8, doi:10.1038/nature10847, URL http://dx.doi.org/10.1038/nature10847, 2012.

Peltier, W.: Global glacial isostasy and the surface of the ice-age Earh: the ICE-5G (VM2) Model and GRACE, Annu Rev Earth Planet Sci, 32, 111–149, doi:10.1146/annurev.earth.32.082503.144359, URL http://www.annualreviews.org/doi/abs/10.1146/annurev.earth.32.082503.144359, 2004.

Radic, V. and Hock, R.: Regionally differentiated contribution of mountain glaciers and ice caps to future sea-level rise, Nature Geosci, 4, 91–94, doi:10.1038/ngeo1052, URL http://dx.doi.org/10.1038/ngeo1052, 2011.

Slangen, A. B. A., Katsman, C. A., Wal, R. S. W., Vermeersen, L. L. A., and Riva, R. E. M.: Towards regional projections of twenty-first century sea-level change based on IPCC SRES scenarios, Climate Dynamics, 38, 1191–1209, doi:10.1007/s00382-011-1057-6, URL http://www.springerlink.com/index/10.1007/s00382-011-1057-6, 2011.